Observation of the $\tilde{A}-\tilde{X}$ Electronic Transition of the 1-$C_3H_7O_2$ and 2-$C_3H_7O_2$ Radicals Using Cavity Ringdown Spectroscopy

Sergey J. Zalyubovsky,[†] Brent G. Glover,[†] Terry A. Miller,*[,†] Carrigan Hayes,[‡] John K. Merle,[‡] and Christopher M. Hadad[‡]

Laser Spectroscopy Facility and Department of Chemistry, The Ohio State University, 120 W. 18th Avenue, Columbus, Ohio 43210

Received: September 16, 2004; In Final Form: December 7, 2004

Cavity ringdown spectra of the $\tilde{A}-\tilde{X}$ electronic transition of the 1-propyl and 2-propyl peroxy radicals are reported. Spectroscopic assignments are facilitated by implementing several production mechanisms, either isomer-specific or not. Assignments of specific spectral lines to particular conformers of a given isomer are suggested. Observations on the temporal decay of the various species are reported.

1. Introduction

Peroxy radicals are key intermediates in both low-temperature combustion[1−3] and atmospheric hydrocarbon oxidation cycles.[4−6] In the troposphere, hydrocarbons and other volatile organic compounds (RH) are oxidized primarily by OH and produce organic radicals, R, that react with molecular oxygen to form peroxy radicals, RO_2. In the clean atmosphere, organic peroxy radicals undergo self-reaction, cross reactions, or reaction with HO_2 to generate alcohols, carbonyl compounds, and hydroperoxides,[7] which can be involved in a variety of important atmospheric processes.

The reaction of peroxy radicals with NO probably has the most prominent impact on the chemistry of a polluted atmosphere:[8]

$$RO_2 + NO \rightarrow RO + NO_2 \qquad (1)$$

The nitrogen dioxide formed in reaction 1 can be photolyzed by solar radiation to produce oxygen atoms that can combine with molecular oxygen to generate ozone. The reaction of organic peroxy radicals with NO may also form, after rearrangement, alkyl nitrates:

$$RO_2 + NO + M \rightarrow RONO_2 + M \qquad (2)$$

The significance of channel 2 increases rapidly with the size of the R group.[9] The branching ratio between the formation of alkyl nitrate and nitrogen dioxide, k_2/k_1, is $<5 \times 10^{-3}$ for the methyl peroxy radical,[10] whereas for the 2-propyl peroxy and *tert*-butyl peroxy radicals, k_2/k_1 is equal to 0.037 and 0.22, respectively.[9,11,12] Therefore, large peroxy radicals can facilitate the transport of pollutants to remote locations or to the upper troposphere where thermal decomposition or photolysis of alkyl nitrates can release NO_2 and alkoxy radicals to the otherwise clean atmosphere.

Peroxy radicals also play a crucial role in low-temperature combustion. Peroxy radicals produced in the oxidation of alkanes can isomerize to form hydroperoxy alkyl radicals:[13]

$$RO_2^{\bullet} \leftrightarrow {}^{\bullet}QOOH \qquad (3)$$

Further QOOH unimolecular decomposition through OO or CO bond cleavage or reaction of the hydroperoxy alkyl radical with molecular oxygen can result in the production of OH or HO_2 radicals. The formation of the hydroxy and hydroperoxy radicals via the peroxy isomerization reaction leads to propagation and branching combustion channels and plays a pivotal role in autoignition and engine knock phenomena.[3] Internal hydrogen transfer in reaction 3 requires a cyclic intermediate structure; therefore, isomerization reaction 3 is more important for peroxy radicals derived from the longer-chain hydrocarbons. The 1-propyl peroxy radical is the first member of the alkyl peroxy family for which it is possible to form a low-energy, six-membered ring transition state, and the propyl + O_2 reaction was recently proposed as a model system for $RO_2 \leftrightarrow$ QOOH isomerization.[14]

Increasing the number of carbons in the R group increases the structural and functional diversity of organic peroxy radicals. Various isomers and conformers can be formed depending on the branching of the hydrocarbon moiety and orientation of the oxygens with respect to the rest of the molecule. Peroxy radicals are involved in a variety of complex reaction mechanisms that depend on structural form. For example, the self-reaction rate constants for 1-propyl and 2-propyl peroxy radicals have been reported to differ by almost 2 orders of magnitude.[15] Hence, it is very desirable to establish spectroscopic diagnostics for various peroxy structural forms in order to investigate isomer and, possibly, conformer specific kinetic behavior.

The propyl peroxy $\tilde{B}-\tilde{X}$ UV absorption spectrum has been characterized and extensively used to follow propyl peroxy reactions in various kinetics experiments.[4,5] However, the $\tilde{B}$ state is dissociative, and therefore the detection of peroxy radicals via the $\tilde{B}-\tilde{X}$ transition has the major disadvantage of a lack of selectivity. Not only is no vibronic structure available to distinguish among peroxy species, but even shifts in the electronic origin are not readily distinguishable because of the transition breath. It is therefore extremely difficult with the $\tilde{B}-\tilde{X}$ transition to distinguish among peroxy radicals containing different R groups, and it is impossible to separate spectra of isomers and conformers for a particular peroxy radical. Previous work on the spectroscopy of the propyl peroxy ground state is

* Corresponding author. E-mail: tamiller+@osu.edu.
[†] Laser Spectroscopy Facility.
[‡] Department of Chemistry.

10.1021/jp0457850 CCC: $30.25
Published on Web 02/02/2005

limited to the observation of the vibrational spectra of the 2-propyl peroxy radical isolated in an argon matrix.[16]

The low-lying $\tilde{A}-\tilde{X}$ electronic transition has been observed in the 2-propyl peroxy radical using a low-resolution modulation absorption technique.[17] It was also shown previously that cavity ringdown spectroscopy (CRDS) detection of the $\tilde{A}-\tilde{X}$ transition of organic peroxy radicals represents both a sensitive and selective technique for their detection.[18−20] This paper is the first report of our experimental and theoretical investigation of propyl peroxy radicals. The emphasis herein is on the experimental separation and assignment of the isomer specific $\tilde{A}-\tilde{X}$ electronic spectra of the 1- and 2-propyl peroxy radicals. We also present information to evaluate the contribution of various conformers to the spectra based on a detailed computational analysis.

2. Experimental Section

2.1. Near-IR Cavity Ringdown Apparatus. The cavity ringdown setup has been described in detail previously.[19,21] Briefly, IR light was generated by stimulated Raman scattering of dye laser radiation. A Nd:YAG pumped dye laser system (PRO-270, Spectra Physics; Sirah GmbH) was operated at 20 Hz in the 657−584-nm region. The output of the dye laser was focused into a single-pass, high-pressure Raman cell filled with molecular hydrogen. The second Stokes radiation generated in the 1.45−1.14-μm region was separated using several color filters (Corion LL-1000), collimated, and directed to the ringdown cavity. The cavity was formed by two high-reflectivity mirrors (Los Gatos Research) attached to the arms of the flow cell. Mirror sets centered at 1.2, 1.3, and 1.4 μm were used to obtain continuous coverage of the investigated spectral region. Ringdown decays were detected by an InGaAs photodiode (Thor Labs, PDA255) and recorded by a digitizing card for further analysis. Typically, 20−40 waveforms were averaged per data point. Absorption scans were recorded with a 0.25-cm^{-1} laser step size and calibrated using water absorption lines published in the HITRAN database.[22] Gaseous reactants were introduced into the flow cell through calibrated mass flow controllers. Vapor from liquid compounds was propagated into the reaction cell by bubbling nitrogen through the liquid contained in a glass bomb, and the flow of the resulting mixture was controlled by a needle valve.

The photolysis excimer laser was operated at 193 nm, and the rectangularly shaped (13 × 0.5 cm) photolysis beam was directed to the cell through two quartz windows perpendicularly to the ringdown probe beam. The photolysis volume is 15 cm^3, and with a 100 cm^3/s pumping speed and 20-Hz repetition rate, the interrogated gas mixture was completely replaced approximately every third laser shot. A subtraction procedure, described elsewhere,[19] was implemented to eliminate background precursor absorption. Typically, the excimer laser was fired ~10 μs before the dye laser, and variation of the delay time between probe and photolysis lasers was used to perform kinetic experiments.

2.2. Production and Kinetics of Propyl Peroxy Radicals. Propyl peroxy radicals have been produced using two mechanisms with distinctly different initiation steps. The first initiation step involves the production of both isopropyl and normal propyl radicals by hydrogen abstraction from propane with chlorine atoms:

$$C_3H_8 + Cl \rightarrow \begin{cases} 1\text{-}C_3H_7 + HCl & \text{(a)} \\ 2\text{-}C_3H_7 + HCl & \text{(b)} \end{cases} \qquad (4)$$

where chlorine atoms have been generated by the 193-nm excimer photolysis of oxalyl chloride,

$$(COCl)_2 \xrightarrow{193\ nm} 2Cl + 2CO \qquad (5)$$

The photolysis of oxalyl chloride is an established source of chlorine atoms,[23] and we have used it in the past to generate acetyl peroxy radicals[19] via a similar hydrogen atom abstraction scheme. The choice of the oxalyl chloride over other sources of chlorine atoms is dictated by its large absorption cross section ($\sigma_{OxCl} = 3.8 \times 10^{-18}$ cm^2 at 193 nm)[23] and its photofragmentation dynamics yielding only carbon monoxide as a stable byproduct of the photolysis.[24]

The production of isopropyl and normal propyl radicals in reaction 4 has been the subject of several previous studies. The room-temperature branching ratio between channels a and b in reaction 4 has been reported to vary from 0.92 to 0.75, favoring production of the isopropyl radical.[25,26] The recommended[15] value for the overall rate of reaction 4 is $k_4 = 1.37 \times 10^{-10}$ cm^3 $molecule^{-1}$ s^{-1}. Our experimental concentrations for $(COCl)_2$ and C_3H_8 are 0.5 and 1 Torr, respectively. The 193-nm photon flux reaching the reaction cell is $\sim 1 \times 10^{16}$ cm^{-2}, which results in the production of $\sim 1 \times 10^{15}$ cm^{-3} chlorine atoms. Clearly, the propane concentration is in excess; therefore, the pseudo-first-order half-lifetime for the Cl atoms is 0.15 μs, with the end result that effectively all of the Cl atoms will be converted to a propyl radical product.

A second propyl radical production mechanism used in our experiments is the direct 193-nm photolysis of 1-bromopropane or 2-bromopropane via

$$CH_3CH_2CH_2Br \xrightarrow{193\ nm} 1\text{-}C_3H_7 + Br \qquad (6)$$

$$CH_3CHBrCH_3 \xrightarrow{193\ nm} 2\text{-}C_3H_7 + Br \qquad (7)$$

to yield propyl radicals in an isomer-specific fashion. The reported[27] 193-nm absorption cross sections for 1-bromopropane and 2-bromopropane are $\sigma_{1-PrBr} = 5.96 \times 10^{-19}$ cm^2 and $\sigma_{2-PrBr} = 2.64 \times 10^{-19}$ cm^2, respectively.

The initiation step of propyl radical generation is rapidly followed by peroxy radical production:

$$C_3H_7 + O_2 + N_2 \rightarrow C_3H_7O_2 + N_2 \qquad (8)$$

Under our experimental conditions ($[O_2] = 50$ Torr and $[N_2] = 150$ Torr), reaction 8 is in the high-pressure limit with bimolecular rate constants of 8×10^{-12} and 1.1×10^{-11} cm^3 $molecule^{-1}$ s^{-1} for the normal propyl and isopropyl radicals, respectively.[15] Our kinetic simulation showed that formation reaction 8 will be complete within a few microseconds and that the propyl radical self-reaction and other secondary reactions ($C_3H_7 + Cl$, $C_3H_7O_2 + Cl$, etc.) contribute less than 5% to the peroxy losses on the time scale of production reaction 8. Other channels resulting in the formation of OH and HO_2 radicals have been observed in reaction 8 at elevated temperatures but appear to be negligible at 296 K.[14,28]

Production of the propyl radicals using the hydrogen atom abstraction scheme has several advantages. First, oxalyl chloride has a considerably larger UV absorption cross section compared to that of 1-bromopropane or 2-bromopropane. In addition to that, two chlorine atoms are produced per absorbed UV photon. Accordingly, the photolysis of $(COCl)_2$ is a more efficient source of the propyl radicals by almost a factor of 20. Second, to produce a concentration of 1×10^{15} molecules cm^{-3} propyl

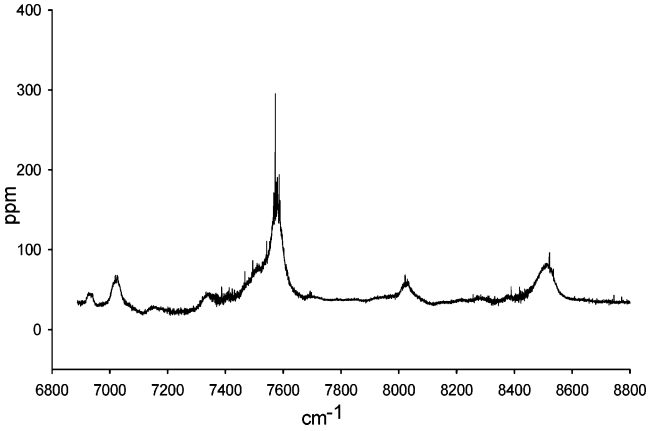

Figure 1. CRDS survey scan obtained with hydrogen atom abstraction from propane in the presence of molecular oxygen. The plotted absorption represents the result of the background subtraction procedure where the difference in CRDS absorption signals with the excimer laser on and off is presented to eliminate precursor and water absorption bands. The time delay between the CRDS probe laser and the photolysis laser is ~10 μs.

radicals with direct photolysis, one needs ~10 Torr of bromopropane into the ringdown cavity compared to only 1 Torr of C_3H_8 in the hydrogen atom abstraction method (assuming identical photolysis conditions). The implication of that is rather significant for the near-IR CRDS. Vibrational overtones and combination bands of CH stretching modes of a stable precursor introduce substantial background absorption into the near-IR ringdown cavity, thereby significantly reducing the sensitivity and dynamic range of the technique.

However, the photolysis of bromopropanes has the advantage of producing only one particular propyl radical isomer, whereas a mixture of isopropyl and normal propyl radicals is generated from reaction 4. Ergo, these two production mechanisms are complementary to each other, and the bromopropane photolysis method is used extensively to identify the carriers of the observed spectra.

For these experiments, oxygen (4.3 UHP grade), nitrogen (6.0 grade), and propane (2.5 grade) were obtained from Praxair. Oxalyl chloride (99%), 1-bromopropane (99%) and 2-bromopropane (99%) were purchased from Aldrich. All reagents were used without further purification.

3. Results and Discussion

Figure 1 shows a survey scan in the 6900−8800-cm^{-1} region obtained with the hydrogen atom abstraction technique. The observed spectrum contains multiple absorption bands with a relatively complex pattern. Contributions from several different sources need to be considered to sort out and assign the observed absorption bands. First, it should be recognized that the scan in Figure 1 represents an absorption spectrum for a mixture of the two different propyl peroxy isomers, normal propyl and isopropyl peroxy radicals. Second, as was described in section 2.1, the photolysis volume was completely refreshed only every third laser shot; therefore, it is possible to observe stable end-reaction products that accumulate in the cell. Consequently, it is necessary to separate the spectrum of the transient species from that of the long-lived products so as to identify the propyl peroxy absorption bands. Thereafter, one can separate the absorptions from those of 1-propyl and 2-propyl peroxy using the photolysis of the corresponding bromopropane isomer with the requirement that the bands have to appear with both the appropriate bromopropane photolysis and the hydrogen-atom abstraction schemes.

3.1. Isolation of the Transient Absorption Signal. To discriminate against stable products, two experimental traces were taken with short (10-μs) and long (30-ms) time delays between the excimer laser and ringdown probe pulses. The resulting scans obtained via photolysis of 1-bromopropane and 2-bromopropane are presented in Figure 2. The intensity of the absorption bands attributable to stable products should remain the same on traces recorded with both short and long delay times, whereas the concentration of the reactive intermediates should be reduced significantly after 30 ms, resulting in weaker absorptions signals. Therefore, one can conclude from Figure 2 that the absorption bands below 7250 cm^{-1} belong to stable species and hence are of no further interest to our propyl peroxy radicals' spectral analyses.

Figure 2 also shows that the time dependence of the bands in the 7250−8600-cm^{-1} region exhibits behavior consistent with the absorption of transient species. Compared to scans with a 10-μs delay time, spectra obtained with a 30-ms delay show absorption bands that are weaker in the case of 2-bromopropane photolysis or nearly absent in the case of 1-bromopropane photolysis.

3.2. Assignment of the Spectra of the Propyl Peroxy Isomers. Theoretical calculations suggest that alkyl group substitution should not significantly affect the nature of the molecular orbitals involved in the peroxy $\tilde{A}-\tilde{X}$ electronic transition.[29] This conclusion is further justified by previous experimental observations[17−19] of the $\tilde{A}-\tilde{X}$ transition of the alkyl peroxy radicals. In addition, good agreement between experimental $\tilde{A}-\tilde{X}$ origin frequencies and values predicted by high-level composite G2 calculations[19] have been reported. Consequently, G2 predictions can serve as an excellent guide for an $\tilde{A}-\tilde{X}$ origin frequency for a given peroxy radical. Therefore, G2 calculations have been performed for C_s symmetric conformers 1-propyl and 2-propyl peroxy radicals. These calculations predict an $\tilde{X}^2A''$ ground state with an $\tilde{A}^2A'$ excited state and $\tilde{A}-\tilde{X}$ separations of 7320 and 7771 cm^{-1}, respectively.

Experimental spectra in the 7300−7700-cm^{-1} and 8200−8600-cm^{-1} regions, generated via hydrogen atom abstraction from propane and photolysis of 1-bromopropane and 2-bromopropane are shown in Figure 3. As one can see, all major absorption bands observed with the photolysis of either 1-bromopropane or 2-bromopropane have counterparts in the spectrum obtained using the hydrogen atom abstraction technique. These band intensities are consistent with branching ratio of 0.92−0.75 for the production of the 1-propyl/2-propyl peroxy radical mixture upon hydrogen atom abstraction from propane as discussed in section 2.2.

Because the $\tilde{A}-\tilde{X}$ electronic transition is essentially a promotion of an electron to the π^* singly occupied orbital localized on the terminal oxygen, one should expect to observe active $\tilde{A}$ state vibrations that involve the terminal oxygen atom. Indeed, all previously observed peroxy radicals exhibit absorption bands assigned to the $\tilde{A}$ state's OO stretching vibration.[17−19,21] Activation of the COO bending vibration has been observed in the $\tilde{A}$ state for the acetyl peroxy radical[19] and in the $\tilde{X}$ state for methyl,[30] ethyl,[30] and *tert*-butyl peroxy radicals.[31] The frequency of the $\tilde{A}$ state's OO stretching vibration varies from 896 cm^{-1} in the hydroperoxy[17] to 932 cm^{-1} in the acetyl peroxy radical,[19] and it is approximately 2−3 times weaker than the electronic origin. Therefore, the peroxy radical's $\tilde{A}-\tilde{X}$ origin band is expected to be accompanied by a satellite $\tilde{A}$ state OO stretching vibrational band shifted roughly by 920 cm^{-1} to the blue, with perhaps a COO bending vibration between.

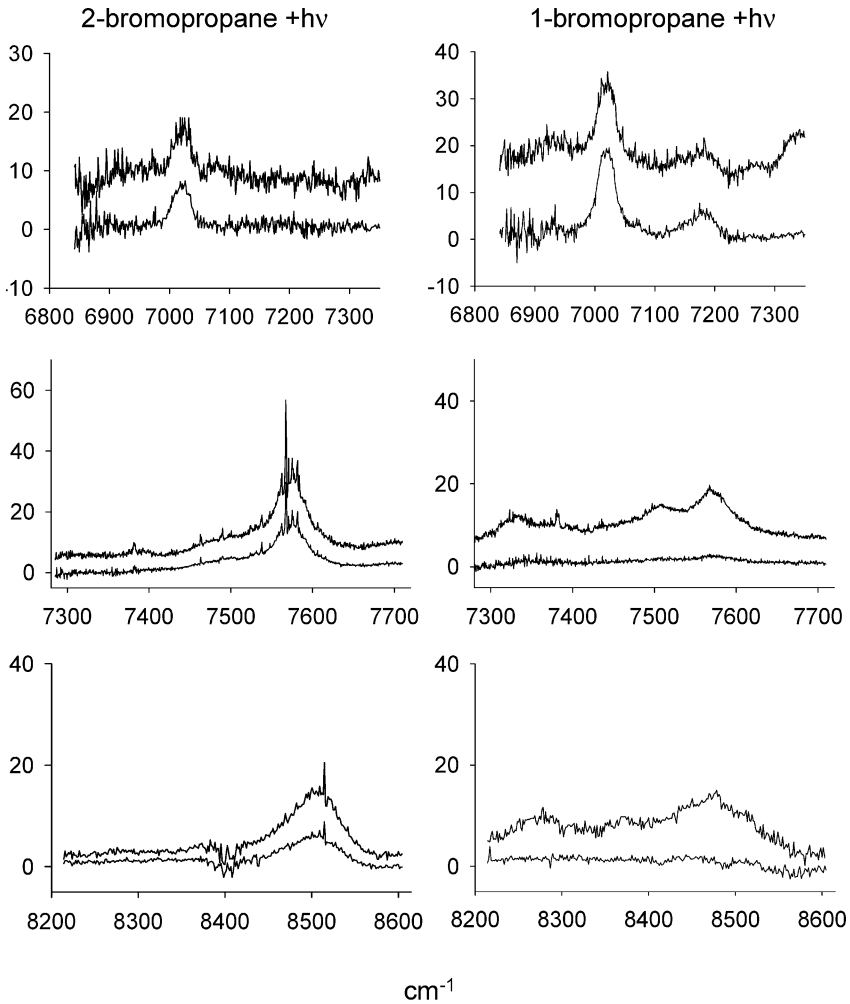

Figure 2. CRDS spectra in three frequency regions of the propyl peroxy radical formed by the photolysis of 2-bromopropane (left) and 1-bromopropane (right). The top trace in each column is recorded within 10 μs of photolysis, whereas the bottom trace is delayed 30 ms.

The absorption spectrum obtained using the photolysis of 1-bromopropane is presented in trace C of Figure 3. Similarities of the absorption contours in the 7300−7700-cm^{-1} and 8200−8600-cm^{-1} regions suggest that the observed bands belong to the same transient species. This conclusion is also supported by the same time-dependent behavior of the absorption spectra shown in Figure 2. Both bands, in the 7300−7700-cm^{-1} and 8200−8600-cm^{-1} regions, vanish after a 30-ms delay. Moreover, the shift between these sets of bands is approximately 900 to 950 cm^{-1}, which is consistent with typical peroxy Ã state OO stretching frequencies. Similar arguments can be applied to the absorption spectrum obtained with the photolysis of 2-bromopropane shown in trace B of Figure 3 (i.e., (i) bands in the 7300−7700-cm^{-1} and 8200−8600-cm^{-1} regions have a close resemblance, (ii) they have similar kinetic behavior, and (iii) the 8200−8600-cm^{-1} band is appropriately blue shifted for an OO stretch).

The agreement between positions of the observed absorption bands with predicted frequencies for the Ã−X̃ origin transition via G2 calculations, observation of the Ã state OO stretching vibrational bands, and comparison of the absorption spectra produced by a mixture of 1-propyl and 2-propyl radicals with bands generated in the isomer-specific photolysis of bromopropanes are consistent with the assignment of absorption traces C and B in Figure 3 to the spectra of the 1-propyl peroxy and the 2-propyl peroxy radicals, respectively. The absorption bands in the 7300−7700-cm^{-1} region are attributed to the electronic origin, whereas bands in the 8200−8600-cm^{-1} region are assigned to the OO vibrational band in the excited state. An additional band around 8000 cm^{-1}, shown in Figure 1, but not recorded with the photolysis of bromopropanes because of strong interference from the precursors is tentatively assigned to the COO bending vibration in either the 1- or 2-propyl peroxy radical.

The observed frequencies of the band maxima shown in Figure 3 are given in Table 1. Multiband absorption structure for both 1- and 2-propyl peroxy radicals may have several sources. Similar to the alkoxy radicals,[32] large alkyl peroxy radicals are expected to exist in multiple conformational forms. Our calculations (described below) show that the 1-propyl peroxy radical has five (Figure 4) and the 2-propyl peroxy radical has two unique, stable conformers. The origin frequency for the Ã−X̃ transition should be similar in all conformers of a particular isomer, and the population of the conformers in the X̃ state will play a large role in determining the relative intensities of the spectral bands. Furthermore, a given transition of each conformer may be accompanied by hot bands associated with transitions from ground-state vibrational levels populated at room temperature. Therefore, the resulting unresolved rotational contour will have superimposed contributions from origin transitions of multiple conformers as well as vibrational hot bands.

The possible rotamers of the 1-propyl peroxy radical are shown in Figure 4 and are denoted by gauche and trans torsion angles for the O−O−C−C and O−C−C−C orientations. As noted above, we have performed calculations for the 1-propyl

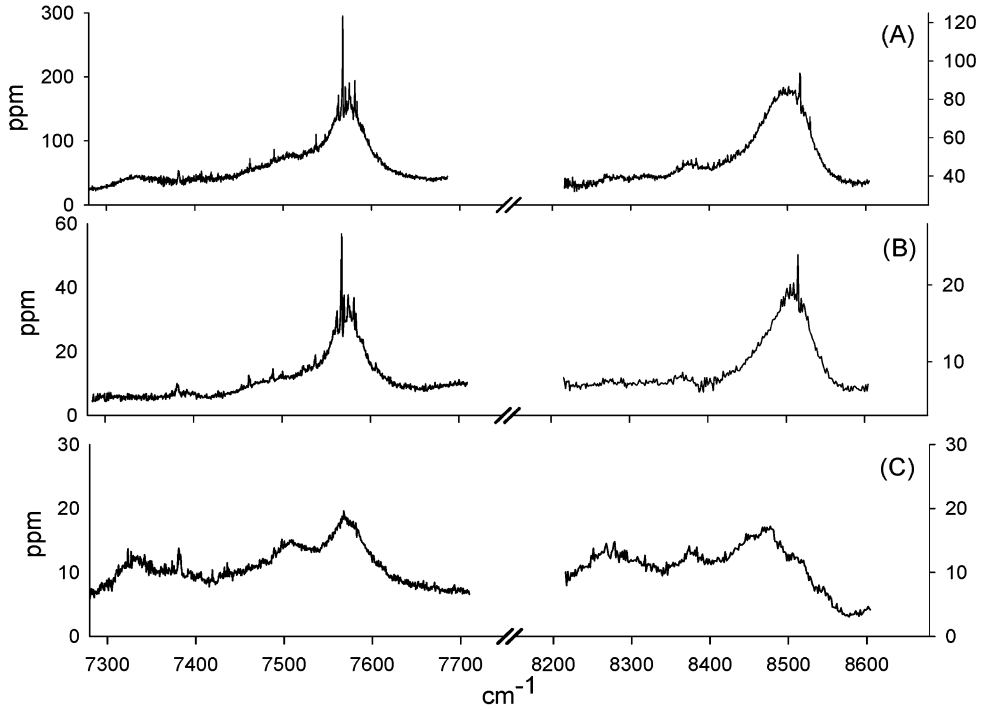

Figure 3. CRDS absorption spectra recorded using the following production mechanisms: (A) hydrogen atom abstraction, (B) 2-bromopropane photolysis, and (C) 1-bromopropane photolysis. The delay time between the excimer laser and CRDS probe is 10 μs.

TABLE 1: Positions of the Observed Band Maxima in cm^{-1}[a]

propyl peroxy isomer	origin region	OO stretching region	separation
1-$C_3H_7O_2$	7332	8273	941
	7508	8380	872
	7569	8474	905
2-$C_3H_7O_2$	7462	8368	906
	7567	8515	948

[a] These band maxima presumably corresponding to different conformers, but as yet the assignment of a given band to a particular conformer (see Table) is uncertain. The uncertainty in the frequencies is $\pm$10 cm^{-1} due to possible overlap of the conformer origin bands and vibrational hot bands.

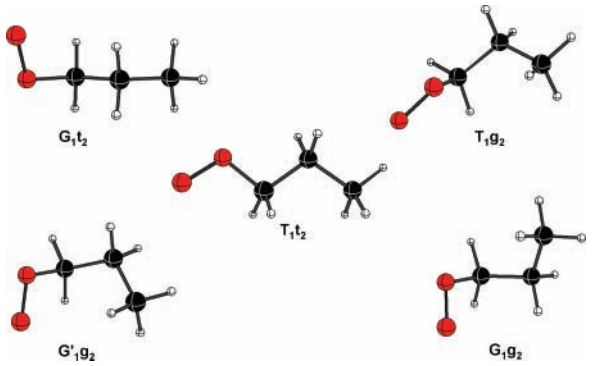

Figure 4. Five possible conformers of the 1-propyl peroxy radical as calculated at the CBS-QB3 level.

and 2-propyl peroxy conformers of C_s symmetry using the Gaussian 98 package,[33] and the results have been used to estimate the $\tilde{A}-\tilde{X}$ origin frequencies for propyl peroxy isomers. Of significant interest was the relative stability of the different rotamers for the 1-propyl peroxy radical (Figure 4). Each of the unique rotamers was calculated at the CBS-QB3,[34] B3LYP/6-31+G**,[35,36] and mPW1K/6-31+G**[37] levels of theory, and each stationary point was confirmed to be a minimum on the potential energy surface via a vibrational frequency analysis. The calculated vibrational frequencies, along with the geometry and the corresponding rotational constants, were also used to estimate the relative free energy at room temperature for the different rotamers. In Table 2, the relative free energies and the resulting Boltzmann distribution (as percentages) for each rotamer are presented. Consistent at all levels of theory, each of the five unique rotamers is calculated to be present at equilibrium in the CRDS experiments. Furthermore, we have also calculated the rotational barriers for interconversion between the different rotamers (via rotation around the C−C and C−O bonds). The rotational barriers are all less than 5 kcal/mol, and hence interconversion is fast at room temperature. Therefore, in agreement with the experiments, at equilibrium a mixture of rotamers is expected, and spectral signatures for different species are observed in the experiments.

TABLE 2: Boltzmann Distributions for Each of the Five Rotamers at the CBS-QB3, B3LYP/6-31+G and mPW1K/6-31+G** Levels along with the Relative Free Energies (ΔG (298 K), kcal/mol) and Conformer Degeneracy**

		CBS-QB3		B3LYP/6-31+G**		mPW1K/6-31+G**	
rotamer	degeneracy	ΔG (298 K)	%	ΔG (298 K)	%	ΔG (298 K)	%
$G_1'g_2$	2	0.41	14.0	0.62	11.8	0.57	11.7
G_1g_2	2	0.00	28.1	0.31	19.8	0.22	21.2
T_1g_2	2	0.04	26.4	0.11	27.8	0.06	28.0
G_1t_2	2	0.21	19.6	0.21	23.7	0.15	23.8
T_1t_2	1	0.10	11.9	0.00	16.8	0.00	15.4

Extensive theoretical calculations for each propyl peroxy conformer are clearly desirable for assigning the observed absorption bands to a particular peroxy conformer because reliable ab initio $\tilde{X}$ and $\tilde{A}$ state energies and vibrational frequencies can be used to predict the origin and hot band transition frequencies as well as their relative intensities. To have a complete picture, the rest of the propyl peroxy conformers of C_1 symmetry have to be theoretically examined and accurate calculations of the excitation energies produced. This

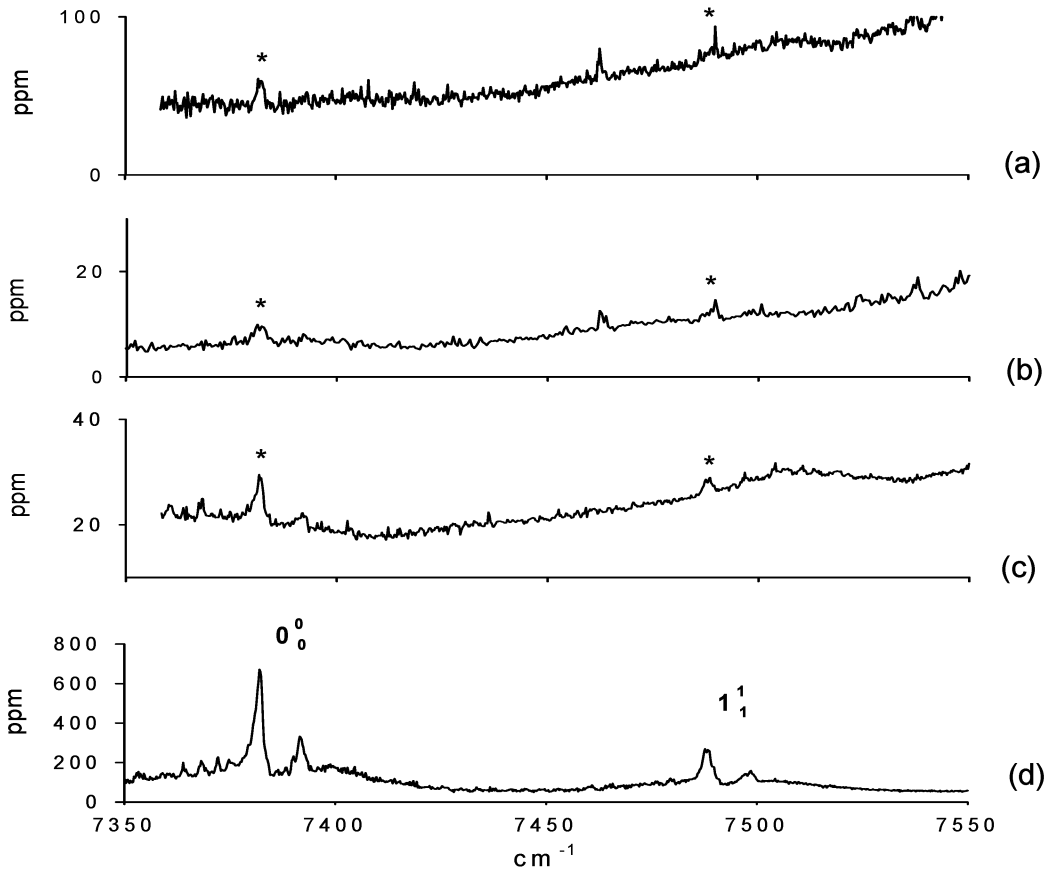

Figure 5. Comparison of the absorption spectra recorded with (a) hydrogen atom abstraction from propane, (b) 2-bromopropane photolysis, and (c) 1-bromopropane photolysis with (d) CRDS spectra of the methyl peroxy radical acquired using acetone as a precursor for methyl radicals.

presents a challenging theoretical problem, but we are presently carrying out such calculations using the equation-of-motion method in the ACESII package and we plan to present these results and corresponding conformer assignments in a forthcoming paper.[38]

3.3. Reaction Dynamics. Figure 2 shows the time evolution of the observed spectra and provides additional confirmation that the absorption bands in traces C and B of Figure 3 belong to the 1- and 2-propyl peroxy radicals. The recommended self-reaction rate constant for the 1-propyl peroxy radical is 3.0×10^{-13} cm^3 molecule^{-1} s^{-1}, which is more than 2 orders of magnitude faster than the reported value of 1.1×10^{-15} cm^3 molecule^{-1} s^{-1} for the 2-propyl peroxy radical.[15] Under the assumption that the second-order self-reaction is the dominant decay channel and using an estimated value of 3×10^{-14} mol/cm^3 as an initial radical concentration, one can estimate half-lives for the peroxy radicals. The estimated half-life is 5.5 ms for the 1-propyl peroxy radical, which is in agreement with the complete disappearance of the 1-propyl peroxy radical's spectra after the 30-ms delay shown in Figure 3. The estimated half-life of the 2-propyl peroxy radical is 1.5 s; correspondingly, only a slight decrease in the 2-propyl peroxy bands is observed in Figure 3. The observed decrease in the 2-propyl peroxy radical's signal also shows that considering only the self-reaction mechanism is an approximation when the self-reaction rate constant is small and other processes such as diffusion, pumping losses, and other reactions are also likely contribute to the radical's destruction.

The experimental spectra presented in Figure 3 exhibit several interesting spectroscopic features that require further examination and analysis. One can notice that a weak absorption peak around 7380 cm^{-1} in Figure 3 appears on spectra produced with the photolysis of both bromopropanes and spectra generated with the hydrogen-atom abstraction method. Figure 5 shows expanded portions of the absorption spectra in the 7350−7500-cm^{-1} region obtained via bromopropane photolysis and hydrogen atom abstraction along with the Ã−X̃ absorption spectrum[18] of the methyl peroxy radical. Both the methyl peroxy origin band and torsional hot band coincide in frequency with weak features marked with asterisks in traces a−c of Figure 5. These spectra lead to the unambiguous conclusion that the methyl peroxy radical is generated in all of our production schemes for the 1-propyl and 2-propyl peroxy radicals.

Several possible sources of the methyl peroxy radical can be considered. Photolytic CC bond cleavage in bromopropanes could lead to the production of the methyl radical, although dissociation along the weaker C−Br bond is expected to be the predominant fragmentation channel. In the H-atom abstraction method, the photolysis of propane could possibly generate methyl radicals via CC bond fission. However, exclusion of the oxalyl chloride from the $C_3H_8/(COCl)_2/O_2$ photolysis mixture eliminates the propyl peroxy *and* the methyl peroxy absorption bands. Therefore, one has to conclude that the methyl peroxy radical is formed after the production of propyl radicals.

Immediately after formation, energy-rich propyl radicals could be subject to dissociation or isomerization. Unimolecular decomposition of the isopropyl radical has two channels: production of the H atom and propylene or the methyl radical and ethene.[39,40] Extrapolation of the available high-temperature data shows that at room temperature both channels have comparable reaction rates on the order of 10^{-14} s^{-1}. Dissociation of the 1-propyl radical may result in formation of the methyl radical at elevated temperatures; however, the room-temperature isomerization rate is likewise expected to be extremely slow (*k*

$= 6.8 \times 10^{-10}$ s^{-1}).[41] Therefore, it is highly unlikely that a 1-propyl or 2-propyl unimolecular dissociation process at room temperature will contribute to methyl radical production; it should be negligible compared to fast propyl radical reaction with oxygen (pseudo-first-order rate constant of 2.5×10^8 s^{-1} under our conditions).

The most plausible explanation for the appearance of the methyl peroxy spectra is obtained by considering details of the propyl peroxy self-reaction mechanism. The self-reaction of propyl peroxy radicals proceeds through formation of a tetroxide,[4] ROOOOR, and in the case of the propyl peroxy radical, there are several established decomposition pathways:[5]

$$C_3H_7O_2 + C_3H_7O_2 \rightarrow \begin{cases} 2C_3H_7O + O_2 & \text{(a)} \\ C_3H_7OH + C_3H_6O + O_2 & \text{(b)} \end{cases} \quad (9)$$

The branching ratio between the propagation channel (a) and the overall reaction rate k_9 is 0.6 for the 2-propyl peroxy radical.[42] No experimental branching ratio is available in the literature for the 1-propyl peroxy radical's self-reaction, but the recommended value of 0.5 can be taken as a first approximation.[7] The propagation channel (a) will result in the production of 1- or 2-propoxy radicals. Acetone and isopropyl alcohol are formed in the termination channel (b) in the case of the 2-propyl peroxy radical's self-reaction, whereas propanal and *n*-propyl alcohol are produced in the case of the 1-propyl peroxy radical. The photolysis of acetone at 193 nm is an excellent source of the formation of methyl radical,[43] and the photolysis of propanal has the methyl radical as one of the dissociation products.[44,45] Figure 2 has shown that some end products can be accumulated in the reaction vessel from one photolysis pulse to the next. Therefore, the photolysis of propyl peroxy self-reaction products may well result in the generation of methyl radicals, with corresponding conversion to the observed methyl peroxy radical.

4. Conclusions

The near-IR $\tilde{A}-\tilde{X}$ electronic transition of propyl peroxy radicals has been observed for the first time by CRDS. The spectra of the two isomeric forms, 1-propyl peroxy and 2-propyl peroxy radicals, have been assigned. These assignments were made with the aid of multiple means of radical production. A less efficient, but isomer-specific, method involved the photolysis of the corresponding bromopropane isomers. Considerably more intense spectra were obtained using $(COCl)_2$ as a "photosensitizer" with hydrogen atom abstraction by Cl producing a mixture of propyl radicals that subsequently reacted with O_2 to produce both propyl peroxy radicals. Spectra were recorded and frequencies were determined for the origin region, the OO stretch, and for the weak COO bend of the $\tilde{A}-\tilde{X}$ electronic transition. Multiple lines were observed, at least some of which must be attributed to different conformers of each isomer. Using high-level ab initio and density functional theory methods, the calculated energies of the five unique conformers of the 1-propyl peroxy radical are very similar, and at equilibrium, a mixture of all five conformers will be present. Furthermore, isomerization barriers between these conformers are small (<5 kcal/mol).

In addition to the spectroscopic conclusions, rudimentary kinetic observations were performed. The much more rapid disappearance of the 1-propyl peroxy radical as compared to that of the 2-propyl peroxy radical is consistent with the reported much larger rate constant for the self-destruction of the primary propyl peroxy isomer. Moreover, for all schemes to generate the propyl peroxy radicals, production of the methyl peroxy radical was also observed. It is suggested that these observations are consistent with the production of acetone or propanal in the propyl peroxy self-destruction reaction. Subsequent photolysis of the ketone or aldehyde produces the methyl radical, which upon reaction with O_2 yields the methyl peroxy radical.

Future work includes assigning the origin bands (and OO stretches) to the specific conformers of the two propyl peroxy isomers observed. Once the details of the CRDS $\tilde{A}-\tilde{X}$ spectral diagnostic are clarified, it can be used to follow the reactions of the peroxy radicals in a species-, isomer-, and even conformer-specific manner. This diagnostic should allow the measurement of cross-reaction rate constants between different organic peroxy radicals.

Acknowledgment. We gratefully acknowledge the support of this work by the National Science Foundation via the Environmental Molecular Science Institute (grant CHE-0089147) and in part via the National Science Foundation (grant no. 0211281). We also thank the Ohio Supercomputer Center for generous computational resources.

References and Notes

(1) Wang, S.; Miller, D. L.; Cernansky, N. P.; Curran, H. J.; Pitz, W. J.; Westbrook, C. K. *Combust. Flame* **1999**, *118*, 415.

(2) Curran, H. J.; Gaffuri, P.; Pitz, W. J.; Westbrook, C. K. *Combust. Flame* **1998**, *114*, 149.

(3) Westbrook, C. K.; Pitz, W. J.; Leppard, W. R. *SAE Technical Paper Series*, International Fuels and Lubricants Meeting and Exposition, Toronto, Canada, Oct 7−10, 1991.

(4) Lightfoot, P. D.; Cox, R. A.; Crowley, J. N.; Destriau, M.; Hayman, G. D.; Jenkin, M. E.; Moortgat, G. K.; Zabel, F. *Atmos. Environ.* **1992**, *26*.

(5) Wallington, T. J.; Dagaut, P.; Kurylo, M. J. *Chem. Rev.* **1992**, *92*, 667−710.

(6) Frost, G. J.; Ellison, G. B.; Vaida, V. *J. Phys. Chem. A* **1999**, *103*, 10169−10178.

(7) Lesclaux, R. Combination of Peroxyl Radicals in the Gas Phase. In *Peroxyl Radicals*; Alfassi, Z. B., Ed.; John Wiley and Sons: New York, 1997; p 92.

(8) Crutzen, P. J. Ozone in the Troposphere. In *Composition, Chemistry, and Climate of the Atmosphere*; Singh, H. B., Ed.; Van Nostrand Reinhold: New York, 1995; p 349.

(9) Atkinson, R.; Aschmann, S. M.; Carter, W. P. L.; Winner, A. M.; Pitts, J. N. *J. Phys. Chem.* **1982**, *86*, 4563.

(10) Pate, C. T.; Finlayson, B. J.; Pitts, J. N. *J. Am. Chem. Soc.* **1974**, *96*, 6554.

(11) Atkinson, R.; Aschmann, S. M.; Carter, W. P. L.; Winner, A. M.; Pitts, J. N. *Int. J. Chem. Kinet.* **1984**, *16*, 1085.

(12) Becker, K. H.; Geiger, H.; Wiesen, P. *Chem. Phys. Lett.* **1991**, *184*, 256.

(13) Walker, R. W.; Morley, C. Basic Chemistry and Combustion. In *Low-Temperature Combustion and Autoignition*; Pilling, M. J., Ed.; Elsevier: Amsterdam, 1997; p 1.

(14) DeSain, J. D.; Klippenstein, S. J.; Miller, J. A.; Taatjes, C. A. *J. Phys. Chem. A* **2003**, *107*, 4415.

(15) Atkinson, R.; Baulch, D. L.; Cox, R. A.; Hampson, R. F.; Kerr, J. A.; Rossi, M. J.; Troe, J. *J. Phys. Chem. Ref. Data* **1997**, *26*, 521−1011.

(16) Chettur, G.; Snelson, A. *J. Phys. Chem.* **1987**, *91*, 913−919.

(17) Hunziker, H. E.; Wendt, H. R. *J. Chem. Phys.* **1976**, *64*, 3488−3490.

(18) Pushkarsky, M. B.; Zalyubovsky, S. J.; Miller, T. A. *J. Chem. Phys.* **2000**, *112*, 10695−10700.

(19) Zalyubovsky, S. J.; Glover, B. G.; Miller, T. A. *J. Phys. Chem. A* **2003**, *107*, 7704.

(20) Atkinson, D. B.; Spillman, J. L. *J. Phys. Chem. A* **2002**, *106*, 8891−8902.

(21) Zalyubovsky, S. J.; Wang, D.; Miller, T. A. *Chem. Phys. Lett.* **2001**, *335*, 298−304.

(22) Rothman, L. S.; Rinsland, C. P.; Goldman, A.; Massie, S. T.; Edwards, D. P.; Flaud, J. M.; Perrin, A.; Camy-Peyret, C.; Dana, V.; Mandin, J. Y.; Schroedera, J.; McCann, A.; Gamache, R. R.; Wattson, R. B.; Yoshino, K.; Chance, K. V.; Jucka, K. W.; Brown, L. R.; Nemtchinov, V.; Varanasi, P. *J. Quant. Spectrosc. Radiat. Transfer* **1998**, *60*, 665−710.

(23) Baklanov, A. V.; Krasnoperov, L. V. *J. Phys. Chem. A* **2001**, *105*, 97−103.

(24) Ahmed, M.; Blunt, D.; Chen, D.; Suits, A. G. *J. Phys. Chem.* **1997**, *106*, 77617−77624.

(25) Tyndal, G. S.; Orlando, J. J.; Wallington, T. J.; Dill, M.; Kaiser, E. W. *Int. J. Chem. Kinet.* **1997**, *29*, 43.

(26) Tschuikow-Roux, E.; Yano, T.; Niedzielski, J. *J. Chem. Phys.* **1985**, *82*, 65.

(27) Kozlov, S. N.; Orkin, V. L.; Huie, R. E.; Kurylo, M. J. *J. Phys. Chem. A* **2003**, *107*, 1333−1338.

(28) DeSain, J. D.; Clifford, E. P.; Taatjes, C. A. *J. Phys. Chem. A* **2001**, *105*, 3205−3213.

(29) Weisman, J. L.; Head-Gordon, M. *J. Am. Chem. Soc.* **2001**, *123*, 11686−11694.

(30) Blanksby, S. J.; Ramond, T. M.; Davico, G. E.; Nimlos, M. R.; Kato, S.; Bierbaum, V. M.; Lineberger, W. C.; Ellison, G. B.; Okumura, M. *J. Am. Chem. Soc.* **2001**, *123*, 9585−9596.

(31) Clifford, E. P.; Wenthold, P. G.; Gareyev, R.; Lineberger, W. C.; DePuy, C. H.; Bierbaum, V. M.; Ellison, G. B. *J. Chem. Phys.* **1998**, *109*, 10293.

(32) Gopalakrishnan, S.; Zu, L.; Miller, T. A. *J. Phys. Chem. A* **2003**, *107*, 5189.

(33) Frisch, M. J.; Trucks, G. W.; Schlegel, H. B.; Scuseria, G. E.; Robb, M. A.; Cheeseman, J. R.; Zakrzewski, V. G.; Montgomery, J. A.; Stratmann, R. E.; Burant, J. C.; Dapprich, S.; Millam, J. M.; Daniels, A. D.; Kudin, K. N.; Strain, M. C.; Farkas, O.; Tomasi, J.; Barone, V.; Cossi, M.; Cammi, R.; Mennucci, B.; Pomelli, C.; Adamo, C.; Clifford, S.; Ochterski, J.; Petersson, G. A.; Ayala, P. Y.; Cui, Q.; Morokuma, K.; Malick, D. K.; Rabuck, A. D.; Raghavachari, K.; Foresman, J. B.; Cioslowski, J.; Ortiz, J. V.; Baboul, A. G.; Stefanov, B. B.; Liu, G.; Liashenko, A.; Piskorz, P.; Komaromi, I.; Gomperts, R.; Martin, R. L.; Fox, D. J.; Keith, T.; Al-Laham, M. A.; Peng, C. Y.; Nanayakkara, A.; Gonzalez, C.; Challacombe, M.; Gill, P. M. W.; Johnson, B.; Chen, W.; Wong, M. W.; Andres, J. L.; Gonzalez, C.; Head-Gordon, M.; Replogle, E. S.; Pople, J. A. *Gaussian 98*, revision A.7; Gaussian, Inc.: Pittsburgh, PA, 1998.

(34) Montgomery, J. A.; Frisch, M. J.; Ochterski, J. W.; Petersson, G. A. *J. Chem. Phys.* **1999**, *110*, 2822.

(35) Becke, A. D. *Phys. Rev. B* **1998**, *98*, 5648.

(36) Lee, C.; Yang, W.; Parr, R. G. *J. Chem. Phys.* **1998**, *37*, 785.

(37) Lynch, B. J.; Fast, P. L.; Harris, M.; Truhlar, D. G. *J. Phys. Chem. A* **2000**, *104*, 4811.

(38) Tarczay, G.; Zalyubovsky, S.; Miller, T. A. To be submitted for publication.

(39) Konar, R. S.; Marshall, R. M.; Purnell, J. M. *Trans. Faraday Soc.* **1968**, *64*, 405−413.

(40) Seakins, P. W.; Robertson, S. H.; Pilling, M.; Slagle, I. R.; Gmurczyk, G. W.; Bencsura, A.; Gutman, D.; Tsang, W. *J. Phys. Chem.* **1993**, *97*, 4450−4458.

(41) Bencsura, A.; Knyazev, V. D.; Xing, S.-B.; Slagle, I. R.; Gutman, D. *Symp. Int. Combust. Proc.* **1992**, *24*, 629−635.

(42) Kirsch, L. J.; Parkes, D. A.; Waddington, D. J.; Woolley, A. *Trans. Faraday Soc.* **1979**, *75*, 2678.

(43) Lightfoot, P. D.; Kirwan, S. P.; Pilling, M. J. *J. Phys. Chem.* **1988**, *92*, 4938−4946.

(44) Chen, Y.; Zhu, L. *J. Phys. Chem. A* **2001**, *105*, 9689.

(45) Heicklen, J.; Desai, J.; Bahta, A.; Harper, C.; Simonaitis, R. *J. Photochem.* **1986**, *34*, 117.